Comparison of Theoretical and Flight-Measured Ionization in a Blunt Body Re-Entry Flowfield

P. W. Huber,* J. S. Evans,† and C. J. Schexnayder Jr.†
NASA Langley Research Center, Hampton, Va.

Plasma diagnostic data from onboard Langmuir probes, reflectometers, and antenna VSWR, along with passive data from attenuation of beacon and telemetry signals, have been obtained for two RAM-C re-entries at orbital velocity. These data are compared with calculations of flowfield ionization and RF signal attenuation for pure air finite-rate nonequilibrium shock-layer and boundary-layer flow, and for boundary layer contaminated with alkali ablation products in local ionic equilibrium. The results show strong effects of ambipolar electron-ion diffusion at high altitude and of ablation impurities at medium and low altitudes. The fast NO^+ recombination rate is indicated.

Nomenclature

A_s = surface area
d_N = hemispherical nose diameter
F = fraction of alkali contaminant in heat shield
f = signal frequency
k = rarefaction parameter, Eq. (4)
M = molecular weight
$\dot{m}$ = surface flux of ablation gases
m_{abl} = ablation mass flow in boundary layer
N_e = electron concentration, cm^{-3}
T = temperature, °K
u = flow velocity
x = distance from nose, along axis
y = distance from body surface, along normal
Γ = reflection coefficient
γ = specific heat ratio
δ = edge of boundary layer
μ = viscosity
ν = electron collision frequency
ρ = gas density
ω = angular signal frequency, $2\pi f$

Subscripts

1,2,3,4 = reflectometer body stations, Table 1
abl = ablation
alk = alkali species
cr = critical value, $N_{e,cr} = (f/8980)^2$
p = peak value at given body station
s = normal shock
w = wall
∞ = ambient flight conditions

Introduction

THE free electrons which are produced in hypersonic flowfield plasmas are the dominant factor in the entry radio blackout phenomenon. Therefore, in order to define, circumvent, or alleviate the blackout problem, it is important that one first be able to determine the magnitude and distribution of electrons in the plasmas near the communications antennas, as well as to determine the interactions which occur between the plasma, the antennas and the propagating electromagnetic signals. The prediction of electron density levels and profiles for a vehicle and trajectory of interest typically requires precise and detailed consideration of complex systems of chemical and thermodynamic processes for the complete shock layer, since free electrons emerge as only trace species in time-dependent systems.[1] Even with careful analysis, uncertainties in the flow species to be considered, the reaction rate coefficients, viscous interactions, antenna near-field effects, etc., contribute to uncertainties in predictions for many real-life situations, particularly those involving ablation contamination[2] or high-altitude blackout.

One purpose of the Langley Research Center Project RAM (Radio Attenuation Measurement) program is to obtain entry flight data which can be interpreted in terms of flowfield models, electromagnetic wave propagation, and alleviation of signal attenuation, to thus aid in verifying or reshaping these models. Flight data are used to supplement laboratory data simply because some facets of the problem cannot be properly simulated on the ground. Toward this end, two RAM-C vehicles of blunted-cone configuration have entered the Earth's atmosphere at near-orbital velocity, near-zero attitude, and with either ablating or nonbalating heat shields. They were equipped with onboard plasma diagnostic sensors, communications systems, and a material injection scheme to modify the plasma and reduce signal attenuation. The ability to draw meaningful conclusions from comparison of flight results and theory lies principally in the fact that data were obtained over a wide range of entry conditions and at several body locations, thus encompassing flow regimes in which different factors are dominant (or negligible).

Description of Flight Experiments

The RAM C-1 and C-2 vehicles were flown in October 1967 and August 1968, respectively, and were both of hemisphere-9° cone configuration. The nose radii were approximately 6 in. (15.25 cm). A complete description of RAM C-1 and its instrumentation, data, etc., is given by Akey and Cross.[3] A similar description of RAM C-2 is given by Grantham.[4] The RAM C-1 heat shield was a phenolic graphite charring ablator (NARMCO 4028) selected for its compatibility with the water injection plasma alleviation experiment. Analysis of this ablator showed that it contained about 1100 μg/g Na. The analysis was incapable of detecting K if present at less than 3600 μg/g, which means that the ablator could contain a maximum of 4700 μg/g of alkali contaminant. RAM C-2 had a Be heat-sink nose cap for the early (prime data period) portion of the entry which was discarded at about 185,000 ft altitude (56.5 km); a teflon ablator was used for the balance of the entry. Both

Presented as Paper 70-756 at the AIAA 3rd Fluid and Plasma Dynamics Conference, Los Angeles, Calif., June 29–July 1, 1970; submitted August 4, 1970; revision received January 27, 1971.

* Head, Flow Field Kinetics Section, Hypersonic Vehicles Division. Member AIAA.

† Aero-Space Technologist, Flow Field Kinetics Section, Hypersonic Vehicles Division.

of these materials were found to be free of any significant amounts of alkali contaminants. Both RAM vehicles had teflon body coatings aft of the heat shields. A sketch of the vehicles and their entry velocity-altitude profile (common to both) is shown in Fig. 1, along with ticks denoting real time values during the flights. During the entry data period, the vehicles had a spin rate of about 3 rps and a near-zero angle of attack, except for a few short periods where it was as high as 5°.

The onboard diagnostic instrumentation for the two entry vehicles is listed in Table 1 and includes a rake of eight Langmuir probes, 15 reflectometers, and four communications antennas. The Langmuir probe experiment[5] was on both of the flights, as were the four antennas, although some of the antennas were at different locations in the two flights. The reflectometer experiment was on RAM C-2 only. The water injection experiment was on RAM C-1 only, and is not discussed herein since correlation of the data with theory is still in progress. However, reduction of signal attenuation was obtained with water injection into the flowfield for the four communications systems used.[3]

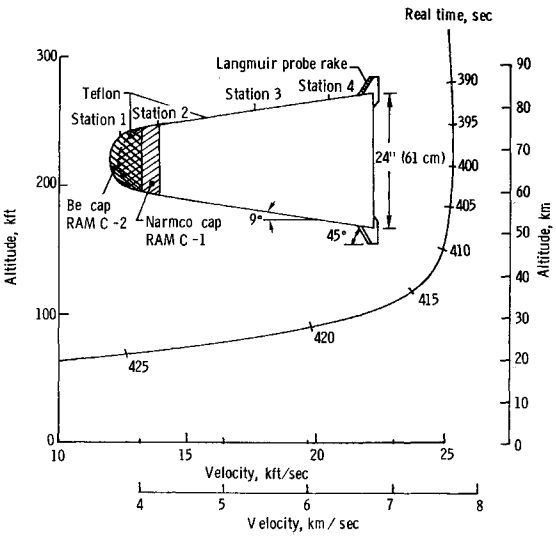

Fig. 1 RAM C configurations and entry profile.

Theoretical Models

Air (Boundary-Layer Regime)

The shock-layer plasma properties for the RAM-C vehicles in the thin boundary layer and vorticity interaction regimes of flight were calculated for pure air by the method of Evans et al.[1] This method uses the streamtube approach (20 streamlines, 54 finite-rate reactions) to calculate the nonequilibrium species concentration in both the inviscid region and the boundary layer. Streamlines are followed into the laminar boundary layer by specifying additional matching conditions on the streamtube as determined from laminar similar solutions. Using iteration techniques and a merging procedure, the method accounts for effects of boundary-layer displacement, streamline swallowing, vorticity interaction normal to the flow direction, and effects of finite rate chemistry on streamline position and shock shape. The principal shortcoming of the streamtube approach for ionization calculations is the inability to include the effects of electron-ion diffusion. Because of this, the method is not applicable to RAM-C at altitudes above about 230,000 ft (70 km), as will be shown later.

Table 1 Location of onboard RF and electrostatic probes

x/d_N[a]	RAM C-1[b]	RAM C-2[b]
0.15 (45°)		K-band reflectometer (35,000)
		X-band reflectometer (10,044)
(Station 1)		S-band reflectometer (3,348)
0.76		K-band reflectometer (35,000)
		X-band reflectometer (10,044)
		S-band reflectometer (3,348)
(Station 2)		L-band reflectometer (1,116)
2.3		K-band reflectometer (35,000)
		X-band reflectometer (10,044)
		S-band reflectometer (3,348)
(Station 3)		L-band reflectometer (1,116)
2.4	VHF telemetry slots (259.7)	
2.6	X-band telemetry horns (9,210)	X-band telemetry horns (9,210)
3.2		VHF telemetry ring (259.7)
3.4	VHF telemetry ring (225.7)	
3.5		K-band reflectometer (35,000)
		X-band reflectometer (10,044)
		S-band reflectometer (3,348)
(Station 4)		L-band reflectometer (1,116)
3.5		C-band beacon horn (5,800)
3.7	C-band beacon horn (5,700)	
3.8		VHF telemetry ring (225.7)
3.9	Langmuir probe rake[c]	
4.0		Langmuir probe rake[c]

[a] Location of centerline of component,
d_N = 12.56 in. (31.90 cm) for RAM C-1, NARMCO
= 12.00 in. (30.48 cm) for RAM C-2, beryllium
= 12.65 in. (32.13 cm) for RAM C-2, teflon.
[b] Frequencies given in MHz.
[c] Probes located at y = 0.96, 1.84, 2.70, 3.58, 4.46, 5.34, 6.20and 7.08 cm.

Contaminated Boundary Layer

Ionization profiles in the RAM C-1 boundary layer are computed also for the case of alkali contaminants in local equilibrium in the air boundary layer. That is, the alkali ionization is assumed to be decoupled from the air-ablation chemistry and is in equilibrium with the local nonequilibrium thermal properties of the air boundary layer as determined previously. No calculations have been made for the teflon-air boundary layer, which is probably electrophillic in nature, since they would primarily apply to the RAM C-2 case at low altitude where the boundary layer is thin relative to the total plasma layer. A reduction of electrons in the boundary layer should only have a minor effect on the radio attenuation through the shock layer.

The input to the RAM C-1 calculation was the flux of vaporized and pyrolyzed NARMCO into the boundary layer along the heat shield surface.‡ In the ablation calculation, transition was assumed to occur at a local Reynolds number of 350,000 (altitude ≈90,000 ft for x/d_N = 0.81, the aft edge of the NARMCO). This flux $\dot{m}$, was then integrated to find the ablation flow rate in the boundary layer at given body locations

$$m_{abl} = \int_0^x \dot{m} dA_s \qquad (1)$$

The value of m_{abl} for x/d_N = 0.81 is also used for all stations downstream of this, since only the NARMCO is considered as a source of alkali contaminants.

The distribution of the ablation gases in the boundary layer is determined next by assuming that they are confined to the boundary layer and that the form of the distribution is the same as that of the velocity defect, for $x/d_N \leq 0.81$. For $x/d_N > 0.81$, the distribution is assumed to progressively

‡ Calculated by E. V. Zoby of Langley Research Center.

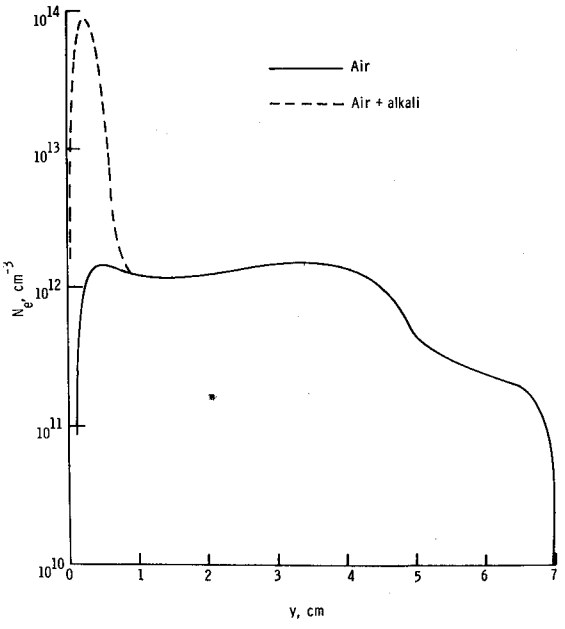

Fig. 2 Electron concentration profiles; x/d_n = 2, altitude = 131,000 ft (40 km).

develop toward one wherein the maximum concentration is located at the point of maximum shear, and wherein the concentration at the wall falls off rapidly as shown by Kemp and Wallace.[6] At all body stations the concentration is assumed to approach a value of zero at the boundary-layer edge. At any given body station the equation

$$m_{\text{abl}}\alpha \int_0^{\delta} (\rho u)_{\text{abl}} dy \tag{2}$$

must, of course, be satisfied.

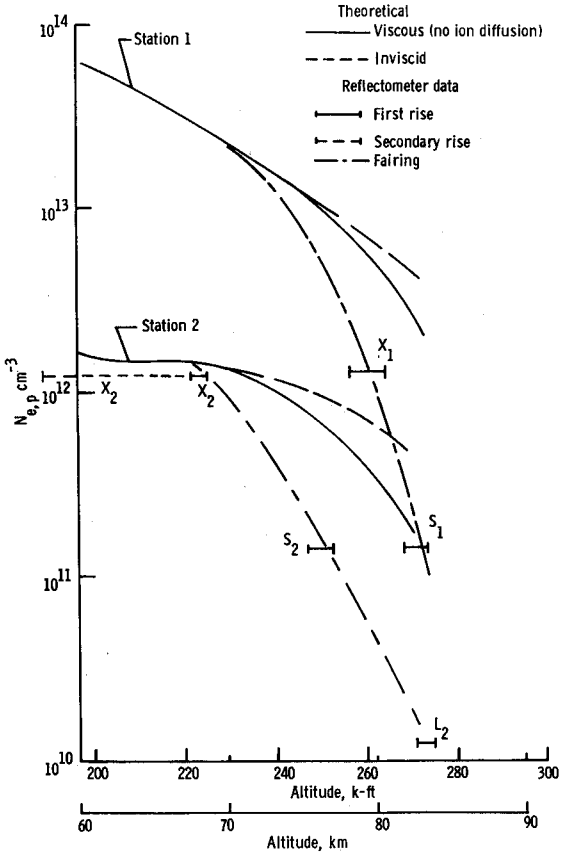

Fig. 3 Comparison of peak electron concentration in the nose region at high altitude.

Given the distribution of ablation gases in the boundary layer $(\rho u)_{\text{abl}}(y)$, from above, and the temperature distribution from the air boundary-layer calculations (where T_w = 1000°K), the Saha equation is used to find the ionization. The mole fraction of alkali species, x_i, used in the Saha equation is related to the ablation gas distribution and alkali contaminant level, F, by

$$x_i(y) = F \frac{M_{\text{abl}}}{M_{\text{alk}}} \frac{(\rho u)_{\text{abl}}/(\rho u)_{\text{air}}}{M_{\text{abl}}/M_{\text{air}} + (\rho u)_{\text{abl}}/(\rho u)_{\text{air}}} \tag{3}$$

where F = 4700 μg/g, the upper limit as determined by the NARMCO analysis. The resulting electron concentration profiles show a large increase in peak N_e due to the above impurity level, as compared with air, as seen in the example plots of Fig. 2.

Use of the local equilibrium assumption probably results in calculated N_e's which are too low at stations aft of the nose, for much of the altitude range, since recombination of the alkali ions is likely to be frozen in the expanding flow. However, use of the upper limit of F may compensate for this to some extent. At high altitudes, the calculated N_e's will be too high due to a probable lag in ion production. The equilibrium assumption was used because the reaction rates for the NARMCO-air mixture are not known, although Anderson and Kendall[7] have made calculations for the case of phenolic carbon. Boundary-layer blowing was not included in the calculation because the blowing parameter (≈0.02, max value) is too small for any significant effects.

Results and Discussion

High Altitude Regime

Peak electron concentration

Profiles of shock-layer electron concentration were computed at various body stations, over a range of altitudes,

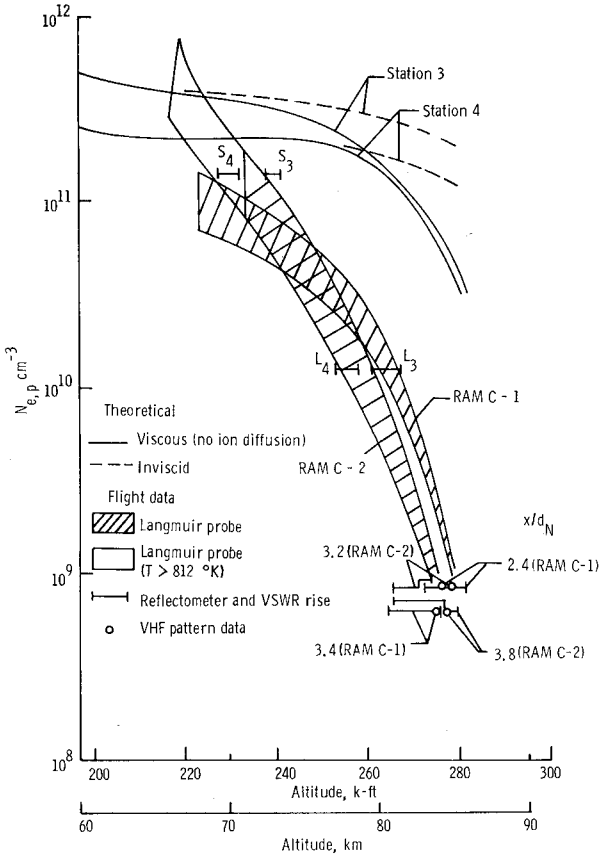

Fig. 4 Comparison of peak electron concentration on the body at high altitude.

both for air, and for air contaminated with alkali species. Values at the peaks of the profiles, $N_{e,p}$, are plotted in Fig. 3 as a function of altitude for body stations 1 and 2 (see Table 1) for the case of pure air. For comparison, peak values are also shown for an inviscid shock layer (before superposition and merging of the boundary layer). The reflectometer data for these body stations are plotted as horizontal bars at values of $N_{e,p} = N_{e,cr}$ for those reflectometers in which a definite rise in reflection coefficient was noted. The length of a bar is representative of the time (altitude) during which the steep part of the rise occurred, and it is assumed that $N_{e,p}$ reached the critical value at some point in this rise. Shock-tube tests of the X- and S-band reflectometers by Taylor[8] indicated that the critical point was at high reflection coefficient (i.e., near the low-altitude ends of the bars). The X_2 record showed a steep partial rise followed by a slower rise to high-reflection coefficient, as shown by the dashed bar. In Fig. 4, the theoretical and experimental data at high altitude for body stations 3 and 4 are shown. In addition to reflectometer data, the rise of VSWR in the VHF antenna feed circuits is shown in a similar manner and can be considered as similar data. The Langmuir probe data shown on Fig. 4 were interpreted from measurements of ion saturation current[3] and the shaded areas represent the envelopes (due to spin and angle of attack) of data from the outermost probes ($y = 7.08$ cm, see Table 1) which represent the highest values measured, although the flight profiles showed no peak. Part of the data for RAM C-2 is shown unshaded and represents that part of the data period where measured probe temperatures exceeded 812°K and were increasing rapidly. The VHF pattern data represents the altitudes at which the antenna patterns (seen because of vehicle spin) were observed to become momentarily circular[9] as predicted by Swift and Knop,[10] for a slightly different antenna array. This occurs for certain types of antennas at the condition $N_{e,p} = N_{e,cr}$ (plasma frequency = signal frequency).

Comparison of theory and flight results in Figs. 3 and 4 brings out some interesting points for discussion. First, it is seen that the theoretical value of $N_{e,p}$ is not greatly reduced by boundary-layer effects below altitudes of about 230,000 ft (70 km) in spite of the fact that the boundary-layer thickness is more than one half the shock-layer thickness at this point. The reason is that, due to nonequilibrium effects, $N_{e,p}$ in the inviscid shock layer is not located near the surface. Second, there is generally good agreement among the various diagnostic techniques shown in Fig. 4. This agreement is particularly impressive with regard to determination of the altitude at which $N_{e,p}$ rises through the critical values for VHF ($N_{e,cr} = 6.3 \times 10^8$ for 225.7 MHz, $N_{e,cr} = 8.4 \times 10^8$ for 259.7 MHz). The pattern data apparently provide a rather precise indication of the critical plasma condition. Third, the slow rise following X_2 in Fig. 3 seems to confirm the theoretical slow rise in $N_{e,p}$ in this same altitude range. Fourth, there does not appear to be any effect of alkali ionization at these altitudes, in view of the agreement of RAM C-1 and C-2 data.

Finally, it is seen that the predictions are much too high (up to two decades) in the altitude range above about 230,000 ft for all the body stations shown, even though the boundary layer does not theoretically fill the shock layer below about 260,000 ft (79 km). As was pointed out previously, however, the theoretical method does not allow for inclusion of electron and ion diffusion effects and is definitely suspect at high altitudes. In order to check this question, correlations of the RAM C data with shock-layer solutions found in the literature, in which ambipolar diffusion and wall recombination effects are included, have been made and are plotted in Fig. 5. The shaded region shown is one which includes theoretically and/or experimentally determined $N_{e,p}$ reduction factors extracted from the results of Lee and Zierten,[11] Kaplan,[12] Kaegi and McMenamin,[13] Kang,[14]

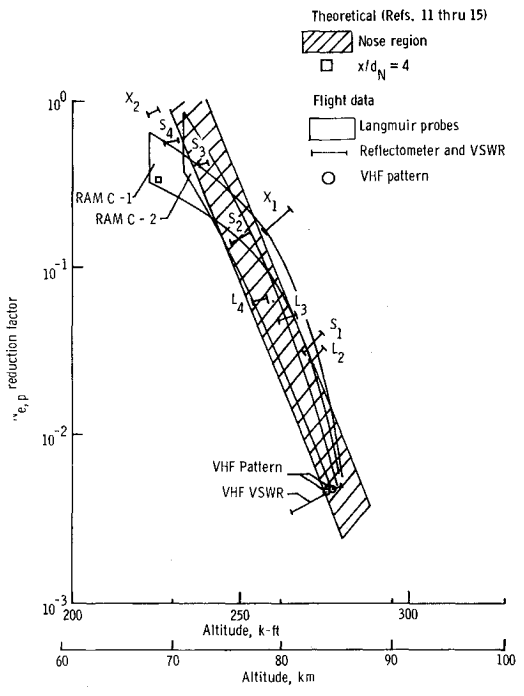

Fig. 5 Correlation of high-altitude data with ion diffusion and wall effects factor.

and Dellinger,[15] and is shown in this manner for simplicity. This is the factor by which $N_{e,p}$ for an inviscid shock layer is reduced due to the effects of viscosity, ion diffusion, and wall recombination. The flight data are divided by $N_{e,p}$ values from the inviscid curves in Figs. 3 and 4. All the reference data are for the nose region of blunt-nosed bodies with the exception of Kaplan[12] which is for $x/d_N = 4$ on a blunt-nosed body. Values appropriate to the stagnation point are generally near the high-altitude side of the shaded region, while values for the nose-body juncture are near the low-altitude side. The data are correlated on the RAM C altitude scale on the basis of the rarefaction parameter,

$$k^2 = [(\gamma_\infty - 1)/2\gamma_\infty](\rho_\infty u_\infty d_N/2\mu_s) \quad (4)$$

and no further corrections are made.

The correlation is seen to be quite indicative of the role of ion diffusion and wall effects in the RAM C shock-layer peak electron concentration. Furthermore, the effects begin at about the altitude predicted ($k^2 \approx 100$), perhaps being shifted in the direction of slightly higher altitudes. There is also a trend toward higher altitudes for the nose region reduction factors as compared with those for aft locations, both in the flight and reference data. With regard to the somewhat different trend of the RAM C-1 Langmuir probe data from the other data, it might be conjectured that the water injection had some adverse effects on the probe. A data dropout occurred for RAM C-1 Langmuir probes starting at an altitude of about 223,000 ft (68 km) and it might also be that the unknown factors leading to this dropout were present to some extent earlier (at higher altitudes).

Electron concentration profiles

There is apparently also a large effect of diffusion and wall recombination on the high altitude N_e profile shape as seen in Fig. 6. The theory shows that $N_{e,p}$ occurs at slightly beyond $y = 4$ cm, while the Langmuir probe determined N_e's are seen to be still increasing at the outermost point, $y = 7.08$ cm. It is to be expected that the wall effects (i.e., surface recombination and gas phase recombination at low temperature and velocity) act as an electron-ion sink and, being fed by diffusion from $N_{e,p}$, will cause a distortion of the profile toward lower $N_{e,p}$ and toward a peak located farther

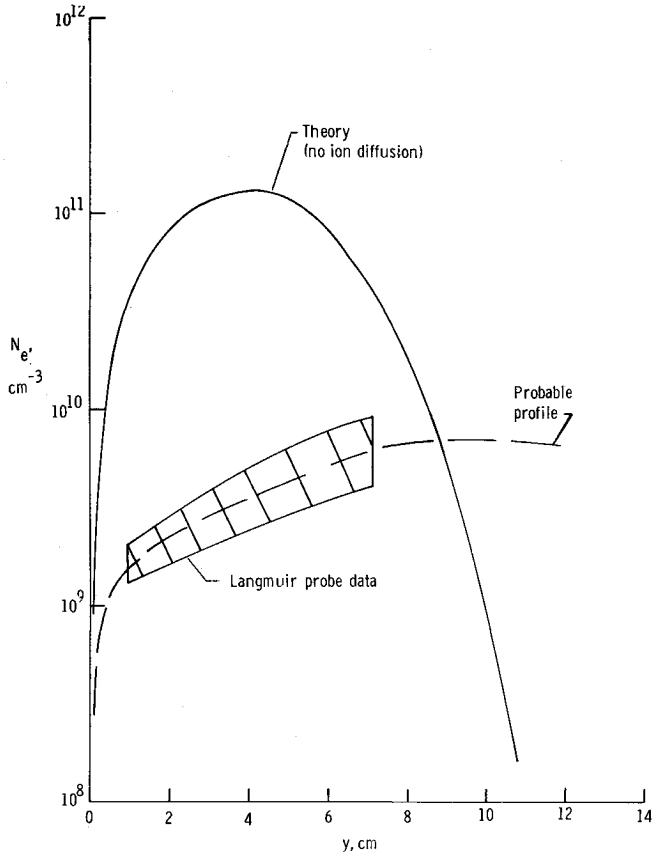

Fig. 6 Comparison of high-altitude electron concentration profiles; x/d_n = 4, altitude = 263,000 ft (80 km).

from the wall. In the outer part of the profile, diffusion reduces the gradients and hence tends to be self limiting, while near the wall the gradients are maintained by the recombination. Furthermore, the outer shock-layer flow at high altitude is producing electrons, even at the aft part of the body, and hence will tend to oppose N_e reduction due to diffusion.

Intermediate Altitude Regime

Signal attenuation

Computer experiments were made to display the sensitivity of the N_e profiles and signal attenuation to the various reaction rates. It was found that in the intermediate altitude range, where X-band and C-band attenuation data are obtained and are not subject to any large question about plane wave concepts (provided the antenna aperture is of the order of a wavelength), the attenuation of these signals is particularly dependent on the NO^+ dissociative recombination rate. This fact is illustrated in Fig. 7 where the rates of Dunn[16] (fast) and of Lin[17] (slow) were used in computing X-band and C-band attenuation. The RAM C-2 flight measured attenuations are also shown and seen to lie between the two cases, but somewhat closer to the fast rate. However, it should be pointed out that in the theory as shown the electron temperature and gas temperature are assumed equal. If electron temperature is assumed to follow the nonequilibrium vibrational temperature of one of the diatomic molecules, then the two cases are raised to higher attenuations (if nitrogen vibration is used,[18] the fast NO^+ case is raised to about where the slow case is shown in Fig. 7, etc.). With this in mind, it would appear that the fast rate is confirmed but that electron temperature may be a little higher than gas temperature (or that interpretation in terms of the plane-wave concept is not completely applicable).

Similar signal attenuation data from RAM C-1 are shown in Fig. 8 for comparison with the contaminated boundary-layer theoretical model. The fast NO^+ rate is used in the inviscid portion of this model and in the pure air case shown for comparison. First of all, comparison of these flight data with that in Fig. 7 shows that the attenuations are definitely higher for RAM C-1. For example, C-band blackout occurs at the altitude where attenuation first began for RAM C-2. Second, the X- and C-band data are in rough quantitative agreement with theory for the lower altitude part of the data period, but drop off markedly at higher altitudes wherein the theory is rising (due to increasing boundary-layer temperature). These discrepancies will be discussed in the next section.

Peak N_e

In order to make comparison of theory with flight data on an $N_{e,p}$ basis and also allow for comparison with the reflectometer data, the attenuations from Figs. 7 and 8 are converted to "deduced $N_{e,p}$" and plotted in Fig. 9. These deduced values are derived by assuming a generalized profile shape (as a function of altitude), and arbitrarily letting the N_e magnitude vary. Values of $N_{e,p}$ are then found whose profiles yield theoretical attenuations equal to the measured attenuations. Theoretical attenuations are computed using the plane wave nonhomogeneous plasma program of Swift and Evans.[19] The shapes assumed in this method are the theoretical shapes previously found (e.g., Fig. 2) where the sensitivity to shape is found by trying different types (pure air fast and slow NO^+, alkali, etc.). Comparison of the pure air results in Fig. 9 leads to the conclusion previously drawn in regard to the NO^+ rate, and is, in fact, strengthened by the reflectometer data (remembering that the low-altitude end of the rise bar is appropriate). For the RAM C-1 data display, the alkali-type shapes are used; however, it was found that the results are not sensitive to shape at the high-altitude ends of the data periods. These results seem to indicate, therefore, that alkali ionization is probably responsible for the difference in observed attenuation between RAM C-1 and C-2, and that the high-altitude fall-off of $N_{e,p}$ at ≈180,000 ft (55 km) is probably due to failure of the local equilibrium assumption in this region, perhaps due to a greatly slowed electron production rate. This data comparison is confirmed also by the high-altitude Langmuir probe data shown previously.

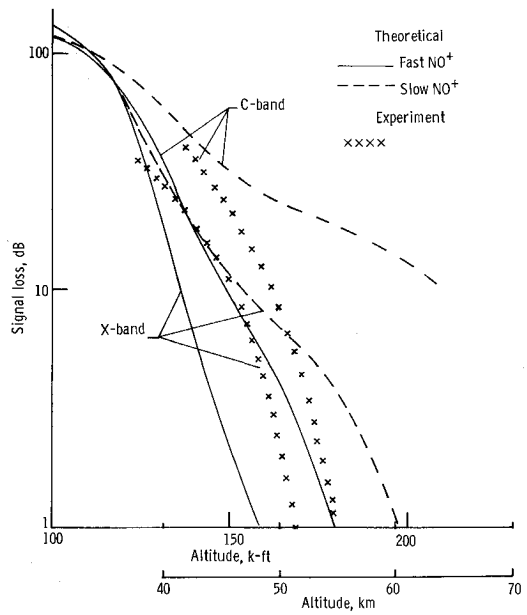

Fig. 7 Comparison of RAM C-2 microwave attenuation data with air theory.

Low-Altitude Regime

Signal attenuation

The low-altitude signal recovery attenuation data for RAM C-1 and C-2 are shown in Fig. 10, plotted as a function of flight velocity (see Fig. 1), for comparison with the theoretical models. Due to a tracking problem, X- and C-band signal recovery data were not obtained for RAM C-2. The comparison brings out a number of interesting points. First, there is a large difference in both theoretical and observed signal attenuation due to the effects of alkali impurities, even though the boundary layer is thin relative to the total plasma layer. This is due to a very large increase in $N_{e,p}$ in the boundary layer at these altitudes (ablation rates are high) due to the impurity. Second, there is very little difference in the predicted recovery altitude as a function of signal frequency for either of the two models. The RAM C-1 data does indeed qualitatively confirm this result for the case of contaminated flow, as there is no particular trend of recovery altitude with frequency. Third, the quantitative agreement of each set of flight data with its respective theoretical model is quite satisfactory considering the many questions and assumptions involved. Boundary-layer transition should have only small effect on the air model (since the boundary layer is thin), while the influence on the alkali model would be to thicken the high N_e spike of the profile (see Fig. 2) probably increasing the attenuation. The local equilibrium assumption should, however, be fairly good for this high-density flow.

Peak N_e

The low-altitude signal attenuation data in Fig. 10 are converted to "deduced $N_{e,p}$" by the method described previously, and plotted in Fig. 11 for comparison with the reflectometer data and the theoretical models. It should be noted that the reflectometer data are shown in two different ways in this figure. The data as interpreted by Grantham[4] are shown by the symbols while the interpretation used herein is shown by horizontal bars plotted at $N_e = N_{e,cr}$, as discussed previously. Grantham assumed that $N_e = 0.63\ N_{e,cr}$ at that point where $\Gamma = 0.20$. Furthermore, some of the data plotted by Grantham are too uncertain in the present interpretation because of several questions due to the effects of ablation, transition, and high collision frequency on the behavior of the reflection coefficient during the decay period. It has been found that these effects can mask the effects of plasma N_e to the degree that meaningful plasma interpretation is not possible. These points are discussed in detail by Schexnayder et al.,[20] and those decays found too uncertain are K_1,K_2,X_1,X_2, and S_1. It is shown here that the increase in peak N_e due to alkali impurity is from 2–3 decades both theoretically and by deduction from the attenuation data. Also, the deduced peak N_e's agree fairly well with the theory for each flight case, as before. However, the most striking result seen in Fig. 11 is that the reflectometer

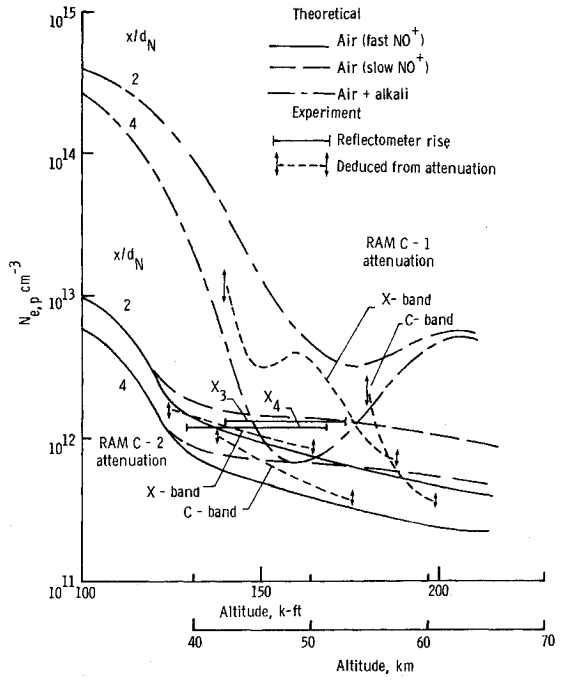

Fig. 9 Comparison of theory with peak electron concentration data at intermediate altitudes.

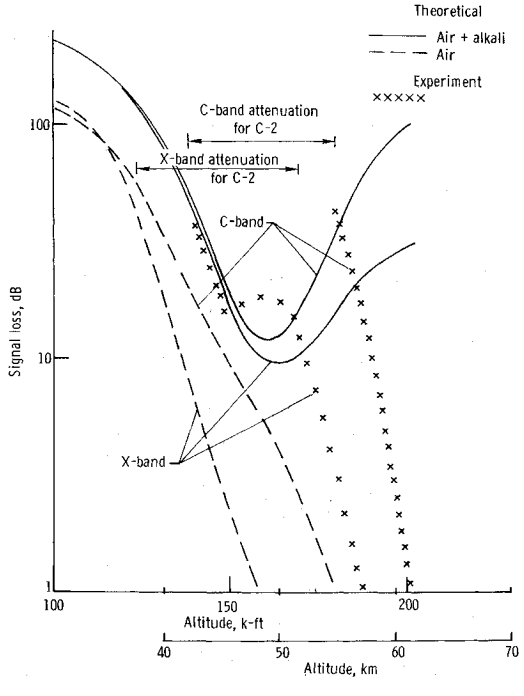

Fig. 8 Comparison of RAM C-1 microwave attenuation data with ablation model.

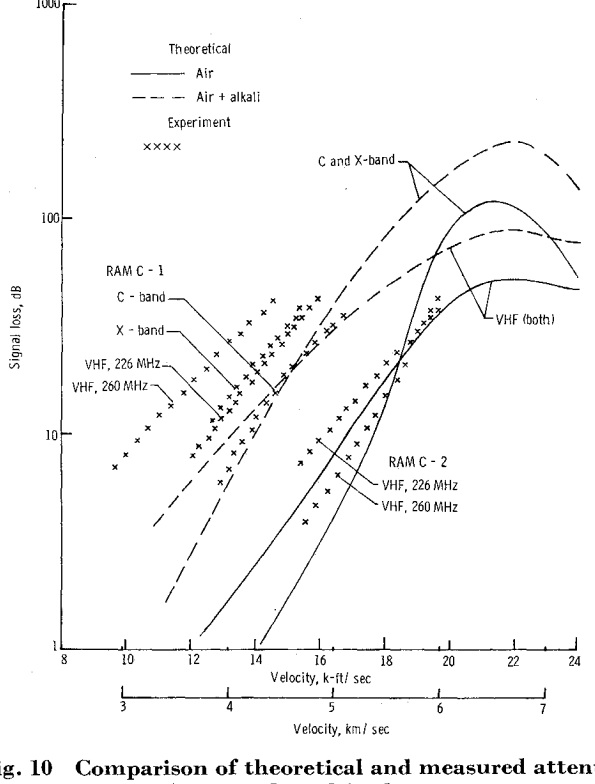

Fig. 10 Comparison of theoretical and measured attenuation at low altitudes.

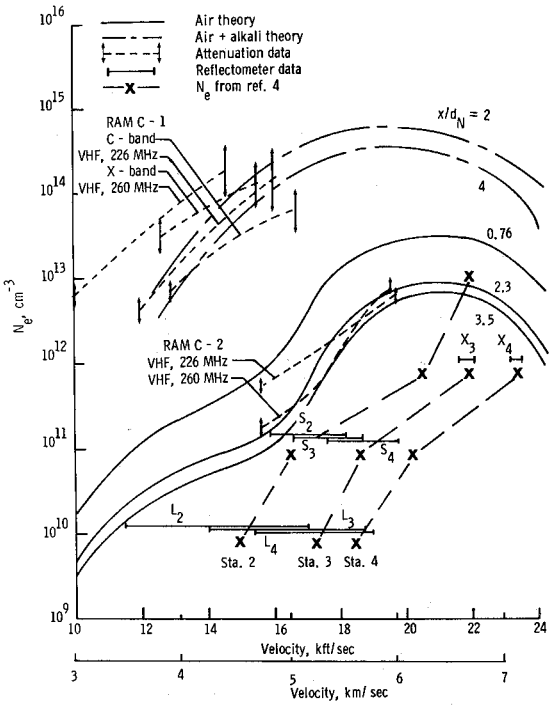

Fig. 11 Comparison of theoretical and experimental peak electron concentration at low altitudes.

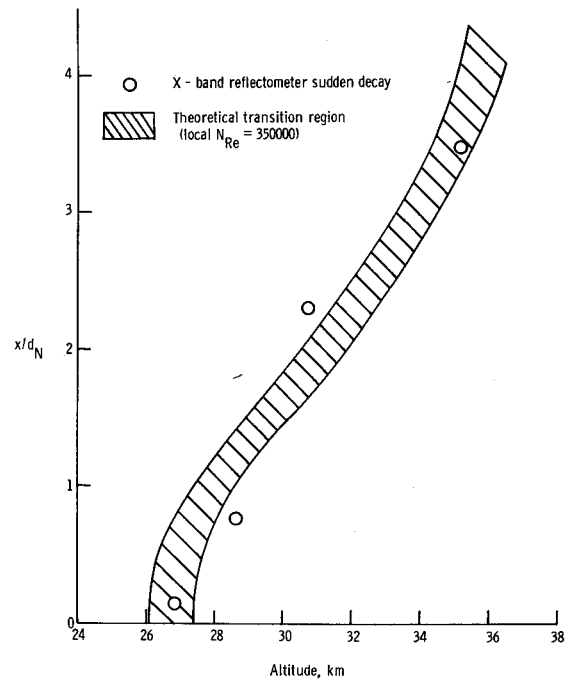

Fig. 13 Correlation of reflectometer decay with boundary-layer transition.

data fall far below the predicted air peak N_e's. The discrepancy is generally about a factor of four, but is as high as seven in the case of S_2 and X_3. However, the discrepancy with Grantham's results is far greater than this.

In the search for an explanation for the contradiction between theory and signal attenuation on the one hand and reflectometer data on the other hand several factors were considered and will be briefly discussed. The first consideration is if both the air theory is wrong and the C-2 VHF attenuation data is incorrectly interpreted. The inviscid prediction cannot be much in error, because this flight regime is one of near-equilibrium as found by computer experiments in which many of the reaction rates were varied, and as confirmed by the calculations for RAM C-2 by Webb et al.[21] The only way the air calculation could be appreciably perturbed would be by the combination of large boundary-layer thickening and chemical action of teflon ablation products. The thickening would presumably occur by the combined effects of early transition, increased mass injection, surface roughness, etc., which must thicken the boundary layer on the nose approximately 10 times the computed laminar value for ablation products to reach the required point in the plasma. This would seem rather unlikely based on the fact that the maximum blowing parameter for the teflon is theoretically only about 0.06, and that material injection studies have

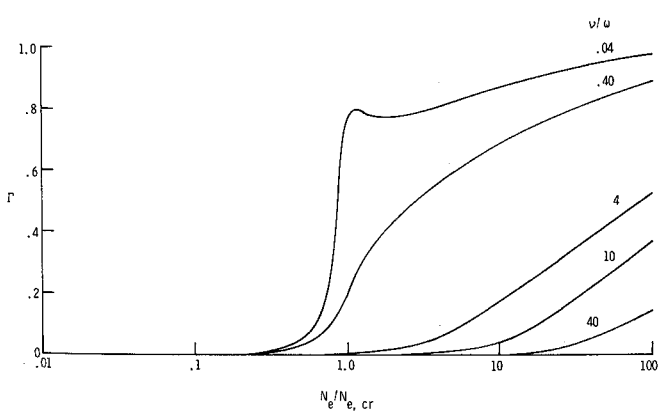

Fig. 12 Theoretical variation of reflection coefficient.

even shown it difficult to cause liquids under pressure to penetrate such high-density flows.

If the teflon could somehow extend this far into the nose-plasma layer, the chemical action required to fit the observations must be either electron attachment or suppressant (interfere with electron production). The computed ablation mass is theoretically about six percent of the mass within the required plasma streamtubes, and DeBolt and Port[22] computed for a five percent teflon-air mixture at about the temperature (6000°K) and density of RAM C-2 nose flow in this regime, that only about one percent of the electrons would be attached, assuming equilibrium (which seems a reasonable assumption). Starner[23] found experimentally that 50 percent teflon-air mixtures did not exhibit attachment for temperatures greater than about 3000°K. Furthermore, the agreement of RAM C-1 low-altitude data with alkali theory tends to rule out any large teflon electrophylic action in the body boundary layer since the body coating theoretically injects more teflon into the boundary layer than there is NARMCO present due to the nose ablation. The alternate possibility of teflon interfering with electron production seems to be equally remote. This would require either lowering the nose flow temperature on the order of 3000°K, or chemically tying up O or N atoms (e.g., CO) to inhibit the reaction $N + O \rightarrow NO^+ + e^-$. Theoretically, there is not nearly enough teflon ablation for this.

The fact that VHF recovery did not occur earlier also tends to rule against the peak N_e indications resulting from the interpretation of the low altitude reflectometer data given in Ref. 4, where the faired peak N_e curves for the aft stations (as a function of altitude) showed decreasing peak N_e below about 23.7 kft/sec (Fig. 11). If such a behavior of peak N_e actually occurred, then this decrease, along with the increasing collision frequency, should result in decreasing attenuation in the region below 23.7 kft/sec (where theoretical peak N_e is increasing) with recovery occurring at least 3 sec earlier than observed (by 22.6 kft/sec).

For the VHF recovery data to be compatible with the reflectometer interpretation given in Ref. 4 for the RAM C-2 flight, there would have to be 25–30 db loss due to antenna mismatch. This is the difference between observed signal loss at recovery and that computed for the reflectometer indicated peak N_e profile (fairing the data in Ref. 4, and then

using plane wave theory and maximum plasma thickness to obtain an upper limit case). However, this would seem to be an unusually high mismatch loss to realize at low altitude where ν is high and reflection losses relatively low. In view of these arguments, it is believed that the VHF attenuation data serves to indicate that the actual peak N_e is closer to the theoretical plasma values than to the low altitude indications from Ref. 4.

However, the best explanation for the discrepancy between plasma theory and reflectometer data appears to be in terms of the generalized reflectometer curves of Fig. 12. For the low altitude reflectometer data used herein the values of ν/ω for S- and L-band were of the order of 1–6, whereas for high altitude they were of the order of 0.01. Reference to Fig. 12 shows that this makes a great deal of difference in the response of the reflectometer. For ν/ω of the order of 0.01, increase of $N_e/N_{e,cr}$ through the value unity causes the reflection coefficient to rise quickly from zero to some large value. However, at the larger values of ν/ω, the reflection coefficient responds much more slowly to increasing $N_e/N_{e,cr}$. Two or more decades of change in $N_e/N_{e,cr}$ are required for the transition between low and high values. This description fits the behavior of the low altitude reflectometer data, since 1) the low-altitude data bars are elongated as compared with the high-altitude ones, and 2) the reflection coefficient descended to small values while $N_e/N_{e,cr}$ was still much larger than unity.

In addition to the influence of high collision frequency on the data plotted herein, the X-band records used by Grantham[4] were noted to have very rapid (nearly discontinuous) decays of reflection coefficient at low altitude. Such behavior is anomalous under high collision frequency conditions and is believed to be associated with transition from laminar to turbulent flow in the boundary layer.

This is illustrated in Fig. 13 where the theoretical altitudes for transition from laminar to turbulent boundary layer (based on a local transition Reynolds number of 350,000) are shown and are compared with transition points as indicated by the X-band decays. The agreement is quite good and leads to the interesting conclusion that the transition for RAM C-2 occurred at fairly low Reynolds number.

As pointed out by Schexnayder et al.,[20] some of these sudden decays in X-band reflection coefficient are not believed to be associated with a sudden drop of peak N_e through the critical value, since the other reflectometers (S- and L-band) located at these same stations showed no such effects.

Conclusions

Comparison of theoretical flowfield plasma properties with those obtained from onboard diagnostic instruments and those deduced from signal attenuation measurements is made for the re-entry regimes of two blunt-nosed vehicles. Results of the comparison lead to the following general conclusions: There is a large effect on both peak concentration and distribution of electrons in the flowfield due to ambipolar electron-ion diffusion and wall recombination, at altitudes corresponding to values of the rarefaction parameter, $k^2 \leq 100$. There is a large increase in electron concentration in the boundary layer due to ionization of alkali impurities from the heat shield, compared to pure air, for altitudes less than about 180,000 ft (55 km). Lack of observed increase at higher altitudes is apparently due to production lag in the alkali species ionization. The fast NO^+ dissociative recombination rate is confirmed, with an indication that electron temperature is somewhat higher than gas temperature in the body flow region. Generally good agreement was obtained between theory, diagnostic data and attenuation data at altitudes greater than 125,000 ft (38 km). At lower altitudes there was reasonable agreement of theory and attenuation data, but disagreement between theory and the diagnostic data. It was shown that the low altitude diagnostic data bars were elongated due to slow response of the reflectometers at high-collision frequency and also that they corresponded to values of $N_e/N_{e,cr}$ well above the value $N_e/N_{e,cr} = 1$.

References

[1] Evans, J. S., Schexnayder, C. J., and Huber, P. W., "Computation of Ionization in Re-entry Flow Fields," *AIAA Journal*, Vol. 8, No. 6, June 1970, pp. 1082–1089.

[2] Blottner, F. G., "Chemically Reacting Boundary Layer With Ablation Products and Nose Bluntness Effects," Rept. 67SD468, June 1967, General Electric Co., Philadelphia, Pa.

[3] Akey, N. D. and Cross, A. E., "Radio Blackout Alleviation and Plasma Diagnostic Results from a 25,000 Foot Per Second Blunt-Body Reentry," TN D-5615, Feb. 1970, NASA.

[4] Grantham, W. L., "Flight Results of a 25,000 Foot-Per-Second Reentry Experiment Using Microwave Reflectometers to Measure Plasma Electron Density and Standoff Distance," TN D-6062, Dec. 1970, NASA.

[5] Jones, W. L., Jr. and Cross, A. E., "Electrostatic Probe Measurements of Plasma Surrounding Three 25,000 Ft/Sec Reentry Flight Experiments," *The Entry Plasma Sheath and Its Effects on Space Vehicle Electromagnetic Systems*, Vol. I, NASA SP-252, 1971, pp. 109–136.

[6] Kemp, N. H. and Wallace, J., "Distribution of a Trace Element in a Boundary Layer with Mass Transfer," *AIAA Journal*, Vol. 8, No. 1, Jan. 1970, pp. 81–87.

[7] Anderson, L. W. and Kendall, R. M., "A Nonsimilar Solution for Multicomponent Reacting Laminar and Turbulent Boundary Layer Flows Including Transverse Curvature," AFWL-TR-69-106, March 1970, Air Force Weapons Lab., Kirtland Air Force Base, N. Mex.

[8] Taylor, W. C., "An Experimental Investigation of the Interaction of Plasmas with Antennas," CR-1727, 1970, NASA.

[9] Croswell, W. F. and Jones, W. F., Jr., "Effects of Reentry Plasma on RAM C-1 VHF Telemetry Antennas," *The Entry Plasma Sheath and Its Effects on Space Vehicle Electromagnetic Systems*, Vol. I, NASA SP-252, 1971, pp. 183–201.

[10] Swift, C. T. and Knop, C. M., "Equatorial Patterns of an Axially Slotted Cylinder Coated with a Critically Dense Plasma," *IEEE Transactions on Antennas and Propagations*, Vol. AP-12, July 1964, pp. 498–502.

[11] Lee, R. H. C. and Zierten, T. A., "Merged Layer Ionization in the Stagnation Region of a Blunt Body," *Proceedings of the Heat Transfer and Fluid Mechanics Institute 1967*, Stanford University Press, Stanford, Calif., 1967, pp. 452–468.

[12] Kaplan, B., "The Nonequilibrium Air Boundary Layer on a Blunt Nosed Body," TIS-67SD227, April 1968, General Electric Space Sciences Lab., King of Prussia, Pa.

[13] Kaegi, E. M. and McMenamin, D. L., Jr., "Measured and Predicted Air Ionization in Blunt Body Shock Layers," AIAA Paper 69-81, New York, 1969.

[14] Kang, S, W., "Analysis of an Ionized Merged-Layer Hypersonic Flow Over a Blunt Body," Rept. AI-2187-A-12, May 1969, Cornell Aeronautical Lab., Buffalo, N.Y.

[15] Dellinger, T. C., "Computation of Nonequilibrium Merged Stagnation Shock Layers by Successive Accelerated Replacement," *AIAA Journal*, Vol. 9, No. 2, 1971, pp. 262–269.

[16] Dunn, M. G. and Lordi, J. A., "Measurement of Electron Temperature and Number Density in Shock-Tunnel Flows. Part II: $NO^+ + e^-$ Dissociative Recombination Rate in Air," *AIAA Journal*, Vol. 7, No. 11, Nov. 1969, pp. 2099–2104.

[17] Lin, S. C. and Teare, J. D., "Rate of Ionization Behind Shock Waves in Air. II. Theoretical Interpretation," *The Physics of Fluids*, Vol. 16, No. 3, March 1963, pp. 355–375.

[18] Lordi, J. A. and Dunn, M. G., "Sources of Electron Energy in Weakly Ionized Expansions of Nitrogen," Rept. AI-2187-A-16, Aug. 1969, Cornell Aeronautical Lab., Buffalo, N.Y.

[19] Swift, C. T. and Evans, J. S., "Generalized Treatment of Plane Electromagnetic Waves Passing Through an Isotropic Inhomogeneous Plasma Slab at Arbitrary Angles of Incidence," TR R-172, Dec. 1963, NASA.

[20] Schexnayder, C. J., Jr., Huber, P. W., and Evans, J. S.,

"Calculation of Electron Concentration for a Blunt Body at Orbital Speeds and Comparison with Experimental Data," TN D-6294, May 1971, NASA.

[21] Webb, H., Jr. et al., "Theoretical Flow Field Calculations for Project RAM," CR-1308, May 1969, NASA.

[22] DeBolt, H. E. and Port, W., "Thermochemical Equilibrium Studies of Ablative Heat-Shield Materials," RAD-TM-63-27, June 1963, Avco Corp., Research and Advanced Development Div., Wilmington, Mass.

[23] Starner, K. E., "Evaluation of Electron Quench Additives in a Subsonic Air Arc Channel," *AIAA Journal*, Vol. 7, No. 12, Dec. 1969, pp. 2357-2358.

JUNE 1971 AIAA JOURNAL VOL. 9, NO. 6

Effects of Electrode Size on the Performance of a Combustion-Driven MHD Generator

E. S. Rubin* and R. H. Eustis†
Stanford University, Stanford, Calif.

Experiments have been conducted to investigate the effects of electrode size on the performance of a combustion-driven MHD generator. Electrode sizes with length-to-pitch ratios of 0.23, 0.50, and 0.79 were tested in a generator section simulated by three molybdenum electrode pairs located at the downstream end of an MHD channel. Voltage probe data were obtained for electrode surface temperatures between 500°K and 1600°K, with gas conductivity in the electrode boundary-layer regions established independently by either a hot (2200°K MgO brick) or cold (750°K water-cooled plate) upstream wall. At a given load current, larger electrodes were found to have lower voltage losses for similar conditions of surface and gas boundary-layer temperature. For dissimilar boundary layers, reflecting coupling between electrode and boundary-layer temperatures in a cold-electrode generator, total voltage losses for a large electrode pair were equal to or greater than those of a small electrode pair at the same surface temperature. Experimental boundary-layer resistances at anodes were in good agreement with analytical predictions based on both an approximate and a more exact gasdynamic model, for electrode temperatures above about 800°K. At lower temperatures anodes were believed to be influenced by solidification of seed compounds on the electrode surfaces, resulting in higher losses. For cathodes, the boundary-layer resistance was gasdynamic for the case of a hot upstream wall, for electrode current densities below that of saturated thermionic emission at the electrode temperature. In all other cases, the presence of cathode surface-sheath effects was indicated.

I. Introduction

SEGMENTED electrodes have long been used in MHD generators to suppress the internal flow of axial currents (associated with the Hall effect) and thereby improve performance relative to the case of a continuous electrode generator. In the one-dimensional idealization of a generator with infinitely fine electrode segmentation, performance is independent of the Hall parameter for typical MHD conditions.[1] In general, however, real segmented generators are at best two-dimensional and the influence of the Hall effect in the presence of finite electrode sizes cannot be ignored.

Besides altering performance because of the Hall effect, finite-length electrodes may also affect MHD generators by influencing the boundary layers which develop along the electrode walls. Boundary layers that are low in temperatures will have a characteristically low electrical conductivity, which may substantially increase the generator's internal resistance.[2] The boundary-layer temperature, however, is coupled to the electrode temperature, and the degree of coupling is dependent on the ratio of electrode length-to-pitch. Thus, for example, one may expect that the characteristic temperature of a boundary layer developing over an electrode wall of small electrodes and large uncooled insulators will remain relatively insensitive to changes in electrode temperature as compared to the case of large electrodes and small insulators, where strong coupling of electrode and boundary-layer temperatures would be expected. Indeed, the presence of such coupling may negate gains in generator performance anticipated on the basis of a fixed conductivity profile. Additionally, electrode size may have an influence on other phenomena typically encountered in MHD generators, such as arc spots and electrode surface-sheath effects. Such phenomena are not well understood and the effects of electrode size in their presence requires study.

Theoretical treatments of the effects of a finite electrode size on MHD generator performance are fairly extensive in the literature for the case of a channel with uniform electrical conductivity.[3-5] Celinsky and Fischer,[5] for example, showed that variation of the electrode length-to-pitch ratio changed the internal resistance by 50% or more (other conditions fixed), and that an optimum electrode size existed which depended on the channel geometry and on the Hall parameter. More recently, MacDonald, Mitchner, and Oliver[6] have

Received June 12, 1970; revision received January 25, 1971. This work was supported by the Air Force Aero Propulsion Laboratory, Wright-Patterson Air Force Base, Ohio. The authors happily acknowledge the many useful conversations with M. Mitchner, C. H. Kruger, and J. F. Louis, and the help of F. L. Levy of the Stanford Plasma Gasdynamic Laboratory.

* Research Assistant, Mechanical Engineering Department; now Assistant Professor, Mechanical Engineering Department, Carnegie-Mellon University, Pittsburgh, Pa. Associate Member AIAA.

† Professor, Mechanical Engineering Department. Associate Fellow AIAA.